Title	Theory of femtosecond coherent double-pump single-molecule spectroscopy : application to light harvesting complexes
Author(s)	Chen, Lipeng; Gelin, Maxim F.; Domcke, Wolfgang; Zhao, Yang
Citation	Chen, L., Gelin, M. F., Domcke, W., & Zhao, Y. (2015). Theory of femtosecond coherent double-pump single-molecule spectroscopy : application to light harvesting complexes. The journal of chemical physics, 142.
Date	2015
URL	http://hdl.handle.net/10220/25478
Rights	© 2015 American Institute of Physics. This is the author created version of a work that has been peer reviewed and accepted for publication by The journal of chemical physics, American Institute of Physics. It incorporates referee's comments but changes resulting from the publishing process, such as copyediting, structural formatting, may not be reflected in this document. The published version is available at: [Article DOI: http://dx.doi.org/10.1063/1.4919240].

Theory of femtosecond coherent double-pump single-molecule spectroscopy: application to light harvesting complexes

Lipeng Chen[1], Maxim F. Gelin[2], Wolfgang Domcke[2], and Yang Zhao*
Division of Materials Science, Nanyang Technological University, 50 Nanyang Avenue, Singapore 639798
[2]*Department of Chemistry, Technische Universität München, Garching D-85747, Germany*

We develop a first principles theoretical description of femtosecond double-pump single-molecule signals of molecular aggregates. We incorporate all singly-excited electronic states and vibrational modes with significant electron-vibrational coupling into a system Hamiltonian and treat the ensuing system dynamics within the Davydov D_1 Ansatz. The remaining intra- and inter-molecular vibrational modes are treated as a heat bath and their effect is accounted for through lineshape functions. We apply our theory to simulate single-molecule signals of the light harvesting complex II. The calculated signals exhibit pronounced oscillations of mixed electron-vibrational (vibronic) origin. Their period decreases with decreasing electron-vibrational couplings.

PACS numbers:

I. INTRODUCTION

Our understanding of the dynamics of complex molecular systems has been shaped, to a considerable extent, by femtosecond nonlinear optical spectroscopy[1–5]. The signals measured by various spectroscopic techniques can be traced back to certain (multi-time) response functions, which contain the information on the material system under study. Notwithstanding insights gained by these investigations, more detailed microscopic information on local molecular motions and fluctuations is needed. The reason is that the responses measured in ensemble experiments are made up of a sum of a large number of transients coming from individual molecules and are thus subject to inhomogeneous broadening and dephasing. The situation is illustrated by the simple formula

$$\frac{1}{\sigma\sqrt{2\pi}}\int d\omega e^{-\frac{(\omega-\omega_0)^2}{2\sigma^2}}\cos(\omega t) = e^{-\frac{\sigma^2 t^2}{2}}\cos(\omega_0 t), \quad (1)$$

which shows how individual oscillatory $\sim\cos(\omega t)$ transients in the time domain produce a rapidly (for $\sigma > \omega_0$ monotonously) decaying response upon ensemble averaging, even if the distribution over the frequencies ω with a characteristic width σ is centered around $\omega_0 \neq 0$. It is thus insightful to overcome ensemble averaging and uncover underlying individual molecular responses.

Information on single molecules is especially vital if we wish to inquire into the dynamics of complex biological aggregates functioning in warm, wet, and noisy environments which cause significant inhomogeneous broadenings of ensemble responses. Shortly after the first proof of principle experiments[6,7], single-molecule spectroscopy has permitted researchers to look behind the fluorescence excitation spectra of light harvesting complex 2 of bacteria (LH2), which is structureless in ensemble experiments, as well as to reveal the excitation pathways[8] and asymmetric fluctuating shapes[9] of LH2. Recent insights into the function of single light harvesting complexes can be found in Refs.[10–13].

Single-molecule experiments have enormously expanded our knowledge base on the structure and functioning of light harvesting complexes. Yet the experiments with continuous-wave lasers, due to the lack of time resolution, deliver only time-averaged responses of individual molecules. Very recently, fluorescence-detection single-molecule spectroscopy has reached a temporal resolution of ~ 10 fs (see Ref.[14] for a recent review). These new single-molecule techniques permit the monitoring in real time of not only electronic populations and vibrational wavepackets, but also of electronic coherences of density matrixes of individual molecules. The techniques have been demonstrated on chromophores (see Ref.[15] for a review) and have recently been applied to reveal long-lived electronic coherences in single LH2 complexes[16].

The simulation and interpretation of femtosecond single-molecule experiments is more challenging for theory than the simulation of ensemble experiment. Generally, femtosecond single-molecule spectroscopy involves strong laser pulses to interrogate individual chromophores[14,15]. Hence the description of their responses requires a non-perturbative treatment of the field-matter interactions[17–19]. Another important issue is a proper description of the dynamics of molecular aggregates. Photosynthetic complexes are characterized by moderate to strong exciton-exciton and exciton-phonon coupling strengths[20–22]. An adequate simulation of the dynamics of such complexes necessitates a non-perturbative treatment of these couplings. The corresponding computational methods are available: The Hierarchy Equation of Motion approach[23–25], the multiconfigurational time-dependent Hartree (MCTDH) method[26–28], hierarchical approximations of the bath spectral density[29,30], or the numerical renormalization group approach[31]. If the system-bath Hamiltonian possesses a certain symmetry, it is possible to derive exact quantum master equations[32,33].

*Electronic address: YZhao@ntu.edu.sg

Yet the application of the methods of Refs.[23–31] to simulate the dynamics of molecular aggregates with multiple strong exciton-exciton and exciton-phonon couplings is beyond the capacity of the present-day computers. We will use a computationally efficient variational approach capable of tackling such systems which is based on the Davydov Ansätze[34–41]. Recently, this approach has been adopted to simulate inter- and intra-ring dynamics in various arrays of molecular rings and yielded accurate results for energy transfer dynamics over a wide range of the exciton-phonon coupling strengths[42,43].

The aim of the present work is the construction of a general theoretical framework for the description of femtosecond double-pulse experiments on single molecular aggregates. We employ the Davydov D_1 Ansatz to simulate femtosecond double-pump signals of single light harvesting complexes II of higher plants (LHCII). The choice of this system is motivated by two reasons. Fundamentally, the understanding of the dynamics of single LHCII complexes is of great importance, since the complex contains more than 50% of the world's chlorophylls[44]. A large body of information on LHCII is available owing to spectroscopic ensemble experiments (see, e.g., Refs.[45,46] and references therein). There exists a microscopic model of the LHCII Hamiltonian which was developed and parameterized in Refs.[47–49]. The model provides a useful first guess of the Hamiltonian for the simulation of single LHCII signals.

Femtosecond single-molecule signals are not yet available for LHCII. The signals simulated for single LHCII complexes cannot be directly related to those reported in Ref.[16] for LH2. Nevertheless, it is instructive to compare the theoretical results for LHCII with the experimental results for LH2 at a qualitative level.

The rest of the paper is organized as follows. In Sec. II, the methodology to calculate the single-molecule signal is elaborated. Sec. III provides an overview of generic time-evolutions of single-LHCII signals. Finally, the conclusions are drawn in Sec. IV.

II. THEORY OF FEMTOSECOND DOUBLE-PULSE SPECTROSCOPY OF SINGLE MOLECULAR AGGREGATES

A. Model system

Consider a molecular aggregate embedded in a dissipative environment. The total Hamiltonian can be written as a sum of the system Hamiltonian, the bath Hamiltonian, and the interaction Hamiltonian,

$$H = H_S + H_B + H_{SB}. \tag{2}$$

We incorporate all electronic states (modeled by two-level systems) and high-frequency vibrational modes with significant electron-vibrational coupling (modeled by harmonic oscillators) into a system Hamiltonian (see, e.g., the discussion in Refs.[50,51])

$$H_S = H_{\rm ex} + H_{\rm ph} + H_{\rm ex-ph}. \tag{3}$$

Here $H_{\rm ex}$ is the Frenkel-exciton Hamiltonian

$$H_{\rm ex} = \epsilon_g|g\rangle\langle g| + \sum_{m=1}^{N}\epsilon_m|m\rangle\langle m| + \sum_{m=1}^{N}\sum_{n\neq m}J_{nm}|n\rangle\langle m|, \tag{4}$$

where $|g\rangle$ and $|m\rangle$ denote the ground state and the mth excited site with energy ϵ_m, respectively, and the J_{nm} are the excitonic couplings. $H_{\rm ph}$ describes the vibrational modes included in the system Hamiltonian

$$H_{\rm ph} = \sum_q \hbar\omega_q b_q^\dagger b_q \tag{5}$$

and $H_{\rm ex-ph}$ is responsible for the intra-molecular electron-phonon coupling which is assumed to be site-diagonal

$$H_{\rm ex-ph} = \sum_q\sum_{m=1}^{N}\chi_{qm}\hbar\omega_q(b_q^\dagger + b_q)|m\rangle\langle m|. \tag{6}$$

Here b_q ($b_q^\dagger$) denotes the annihilation (creation) operator of the phonon with frequency ω_q, and χ_{qm} specifies the coupling of the site m to the phonon mode q. The latter is traditionally quantified by the Huang-Rhys factors $S_{qm} = \chi_{qm}^2$ which can be determined through normal mode analysis.

The third term in Eq. (2) describes interactions of the system with low frequency inter-molecular vibrations which are weakly coupled to the electronic degrees of freedom of the molecular aggregate, as well as with the nuclear degrees of freedom of the environment. Having incorporated the vibrational modes with significant electron-phonon coupling into H_S, we may chose a rather simplified description of the dynamics governed by H_B and H_{SB}. They are responsible for population decays and dephasings at longer time scales. We assume a harmonic bath with site-independent and site-diagonal system-bath coupling[52–54]:

$$H_B = \sum_j \hbar\Omega_j a_j^\dagger a_j, \tag{7}$$

$$H_{SB} = \sum_j\sum_{m=1}^{N}\kappa_j\hbar\Omega_j(a_j^\dagger + a_j)|m\rangle\langle m|. \tag{8}$$

Here a_j ($a_j^\dagger$) is the annihilation (creation) operator of a phonon of the jth bath mode with frequency Ω_j and site-independent system-bath coupling strength κ_j. The bath spectral density is defined as

$$D(\omega) = \sum_j \kappa_j^2\Omega_j^2\delta(\omega - \Omega_j) \tag{9}$$

All parameters specifying the Hamiltonian (i.e. the site energies ϵ_m, the electron-phonon couplings χ_{qm}, and the system-bath couplings κ_j) depend significantly on distances between the pigment molecules bound to the protein scaffold as well as configurations of the solvent[55]. Hence, the Hamiltonian of Eq. (2) is, in fact, a snapshot Hamiltonian. Every single-molecule signal corresponds to a particular realization of the values of ϵ_m, J_{mn}, χ_{qm}, and κ_j sampled from certain distributions.

B. Phase-locked double-pump single-molecule signal

The experiment of van Hulst and coworkers[16] can be viewed as a single-molecule version of the femtosecond double-pump experiment of Scherer *et al*[56,57] in the gas phase. In these experiments, the molecules are excited by two phase-locked laser pulses. We thus define the field-matter interaction Hamiltonian in the dipole approximation and in the rotating wave approximation as follows:

$$H_F(t) = -\lambda[\varepsilon(t)X^\dagger + \varepsilon^*(t)X], \tag{10}$$

where

$$\begin{aligned} \varepsilon(t) &= \varepsilon_1(t) + \varepsilon_2(t), \\ \varepsilon_1(t) &= E(t)e^{-i\omega_1 t}, \\ \varepsilon_2(t) &= E(t-\tau)e^{i(\phi-\omega_2 t)}. \end{aligned} \tag{11}$$

Here λ and $E(t)$ is the amplitude and dimensionless envelope of the pulses, respectively; ω_1 and ω_2 are the pulse carrier frequencies; τ and ϕ are the time delay and the relative phase of the pulses, respectively. The transition dipole moment operator is specified as

$$\begin{aligned} X &= \sum_{m=1}^{N} \boldsymbol{e}\boldsymbol{\mu}_m |g\rangle\langle m|, \\ X^\dagger &= \sum_{m=1}^{N} \boldsymbol{e}\boldsymbol{\mu}_m |m\rangle\langle g|. \end{aligned} \tag{12}$$

Here $\boldsymbol{e}$ is the unit vector defining polarization of the laser pulses and $\boldsymbol{\mu}_m$ is the transition dipole moment between the excitonic ground state $|g\rangle$ and an excited state $|m\rangle$ of site m.

The total material density matrix, which describes the evolution and optical excitation of the molecular aggregate coupled to a heat bath, obeys the Liouville – von Neumann equation

$$\partial_t \rho(t) = -i[H + H_F(t), \rho(t)]. \tag{13}$$

The observable is the total (relaxed) spontaneous emission from the lowest fluorescent state of the molecular aggregate measured as a function of time delay between the two pump pulses[16]. In principle, a proper description of spontaneous emission requires quantization of the electromagnetic field and its detection by time and frequency gating[58,59]. Such a description is not necessary in the present case, since the total fluorescence of the molecular aggregate in the optical domain is proportional to the total population of the manifold of singly-excited excitonic states after the interaction with both laser pulses

$$S(\tau) = \mathrm{Tr}\{\mathcal{P}_1 \rho(t \to \infty)\} \tag{14}$$

where

$$\mathcal{P}_1 = \sum_{m=1}^{N} |m\rangle\langle m|. \tag{15}$$

and trace is taken over all nuclear degrees of freedom.

The signal of Eq. (14) can alternatively be expressed through the total complex nonlinear polarization

$$P(t) = \mathrm{Tr}\{X\rho(t)\} \tag{16}$$

as follows[17]:

$$S(\tau) = -2\,\mathrm{Im}\int_{-\infty}^{\infty} dt\, \varepsilon^*(t) P(t). \tag{17}$$

Eq. (17) can be derived by the multiplication of both sides of Eq. (13) by $\mathcal{P}_1$, integration over time from $-\infty$ to ∞, and taking the trace. Eq. (17) is reminiscent of the formula for the intensity of the integral transient absorption pump-probe signal[2], but differs from it in two respects. (i) $P(t)$ is the total, rather than the phase-matched polarization, and (ii) $P(t)$ is the nonlinear polarization which contains all possible contributions in the system-field interaction λ.

A general nonperturbative theoretical description of the phase-locked double-pump experiment for a homogeneous molecular ensemble has been developed in Ref.[17]. To describe the single-molecule signals, it requires a number of modifications which are explained below.

C. Response functions

The single-molecule signal of Eq. (17) can be expanded in powers of the pulse strength λ,

$$S(\tau) = \sum_{k=1}^{\infty} \lambda^{2k} S_k(\tau). \tag{18}$$

Each contribution $S_k(\tau)$ can be calculated through the corresponding $2k-1$-order response functions[60–62]. The experiment of Ref.[16] was performed with weak laser pulses. The photon fluence was chosen to ensure that the experiment was in the linear regime, so that excited-state absorption and stimulated emission were avoided. We thus may restrict ourselves to the evaluation of the leading contribution $S_1(\tau)$, which is determined by the linear response function and identify $S(\tau)$ with $S_1(\tau)$.

Following the line of reasoning of Ref.[63], we assume that a single-molecule response selects a specific initial state of the system ($\boldsymbol{\xi}_S$) and bath ($\boldsymbol{\xi}_B$) phonons in the ground excitonic state (g), which is randomly sampled according to the Boltzmann equilibrium distribution. Hence, the initial condition for the Liouville – von Neumann equation (13) can be written as

$$\rho(0) = |\boldsymbol{\xi}_B\rangle|\boldsymbol{\xi}_S\rangle|g\rangle\rho^{eq}_{\boldsymbol{\xi}_S\boldsymbol{\xi}_B}\langle g|\langle\boldsymbol{\xi}_S|\langle\boldsymbol{\xi}_B|, \tag{19}$$

where

$$\rho^{eq}_{\boldsymbol{\xi}_S\boldsymbol{\xi}_B} = Z_{\rm eq}^{-1}\langle g|\langle\boldsymbol{\xi}_S|\langle\boldsymbol{\xi}_B|\exp\left\{-\frac{H}{k_BT}\right\}|\boldsymbol{\xi}_B\rangle|\boldsymbol{\xi}_S\rangle|g\rangle \tag{20}$$

($Z_{\rm eq}$ is the partition function, k_B is the Boltzmann constant, and T is a bath temperature). We denote the Hilbert-space vectors for the system and the bath phonons as $|\boldsymbol{\xi}_S\rangle$ and $|\boldsymbol{\xi}_B\rangle$, respectively.

Having specified $\rho(0)$, we can straightforwardly calculate the linear (first-order) contribution to the polarization (16). This yields the following formal expression for the single-molecule signal[17]:

$$S_{\boldsymbol{\xi}_S\boldsymbol{\xi}_B}(\tau) = \sum_{a,b=1}^{2}\sigma^{ab}_{\boldsymbol{\xi}_S\boldsymbol{\xi}_B}(\tau) \tag{21}$$

where

$$\sigma^{ab}_{\boldsymbol{\xi}_S\boldsymbol{\xi}_B}(\tau) = 2{\rm Re}\int_{-\infty}^{\infty}dt\int_0^{\infty}dt_1\varepsilon_a^*(t)\varepsilon_b(t-t_1)R_{\boldsymbol{\xi}_S\boldsymbol{\xi}_B}(t_1) \tag{22}$$

and

$$R_{\boldsymbol{\xi}_S\boldsymbol{\xi}_B}(t) = \rho^{eq}_{\boldsymbol{\xi}_S\boldsymbol{\xi}_B}\langle g|\langle\boldsymbol{\xi}_S|\langle\boldsymbol{\xi}_B|e^{iHt}Xe^{-iHt}X^\dagger|\boldsymbol{\xi}_B\rangle|\boldsymbol{\xi}_S\rangle|g\rangle \tag{23}$$

is the state-specific linear response function or the transition dipole moment correlation function.

A practical implementation of Eq. (23) requires additional approximations:

(i) We assume that the system vibrations are initially in their lowest state $\mathbf{0}_S$. This is a good approximation since characteristic energies of high-frequency optically-active vibrational modes are much higher than k_BT. Therefore, it is unlikely that a single-molecule experiment picks a complex which is in an excited state of one of the high-frequency system modes.

(ii) The bath defined by the Hamiltonian (7) comprises the low frequency slow intra- and intermolecular vibrational modes. The optical excitation of a single molecule does not involve and control the bath vibrations $\boldsymbol{\xi}_B$ which are initially in thermal equilibrium at a temperature T. Then, to a good approximation, the single-molecule signal is independent of the initial state of the bath, and we can perform the summation over the bath vibrational modes, like in ensemble experiments.

Hence, we can approximate the single-molecule response function and the signal as follows:

$$R(t) = \sum_{\boldsymbol{\xi}_B}R_{\mathbf{0}_S\boldsymbol{\xi}_B}(t), \tag{24}$$

$$S(\tau) = \sum_{\boldsymbol{\xi}_B}S_{\mathbf{0}_S\boldsymbol{\xi}_B}(\tau). \tag{25}$$

To explicitly evaluate the bath effect on $R(t)$, we note that the system Hamiltonian (3) commutes with the bath Hamiltonian (7) and the system-bath coupling Hamiltonian (8), $[H_S, H_{SB}+H_B]=0$. The bath-induced relaxation can thus be described by the second-order cumulant contribution[2]. The result reads:

$$R(t) = e^{-g(t)}\sum_{n,n'}C_{n,n'}\langle\mathbf{0}_S|\langle n|e^{-iH_St}|n'\rangle|\mathbf{0}_S\rangle, \tag{26}$$

where

$$g(t) = \int_0^{\infty}d\omega\frac{D(\omega)}{\omega^2} \times\left[\coth\left(\frac{\hbar\omega}{2k_BT}\right)(1-\cos\omega t)+i(\sin\omega t-\omega t)\right]. \tag{27}$$

is the lineshape function.

Eq. (26) contains the geometrical factors

$$C_{n,n'} = (\boldsymbol{e}\boldsymbol{\mu}_n)(\boldsymbol{e}\boldsymbol{\mu}_{n'}), \tag{28}$$

which account for statistical orientations of the pigment molecules in the laboratory frame. We neglect reorientation of the molecules, which is a good approximation on the time scale of a few hundreds of femtoseconds[64,65].

Summarizing, we have arrived at a simple recipe for the calculation of the double-pump signal of a single molecular aggregate. The procedure is like this:

- The parameters specifying the Hamiltonian (i.e., the site energies ϵ_m, the electronic couplings J_{nm}, the electron-phonon couplings χ_{qm}, and the system-bath couplings κ_j) are sampled from certain (for example, Gaussian) distributions.
- The orientation of the aggregate in the laboratory frame is randomly chosen[66,67].
- The single-molecule signal is evaluated for a specific realization of ϵ_m, J_{nm}, χ_{qm}, κ_j, and $\boldsymbol{\mu}_n$.

The corresponding ensemble signal is obtained by the summation over different realizations of the single-molecule signals. The averaging over orientations of the transition dipole moments $\boldsymbol{\mu}_n$ can be performed analytically. It results in the replacement of $C_{n,n'}$ of Eq. (28) by

$$\bar{C}_{n,n'} = (\boldsymbol{\mu}_n\boldsymbol{\mu}_{n'})/3. \tag{29}$$

D. The Davydov Ansatz

We evaluate the system propagator in Eq. (26) by employing the Davydov D_1 Ansatz:

$$e^{-iH_St}|n\rangle|\mathbf{0}_S\rangle = |\Psi_{D_1}(t)\rangle, \tag{30}$$

$$|\Psi_{D_1}(t)\rangle \;=\; \sum_n \alpha_n(t)|n\rangle \exp\left\{\sum_q [\lambda_{nq}(t)b_q^\dagger - H.c.]\right\}|\mathbf{0}_S\rangle. \tag{31}$$

A detailed description of the underlying theory can be found in Refs.[40–43,50]. The time-dependent variational parameters $\alpha_n(t)$ and $\lambda_{nq}(t)$ can be obtained by solving a set of differential equations generated by the Lagrangian formulation of the Dirac-Frenkel variational principle[68]. The equations of motion for these parameters,

$$\frac{d}{dt}\left(\frac{\partial L}{\partial \dot\alpha_n^*}\right) - \frac{\partial L}{\partial \alpha_n^*} \;=\; 0. \tag{32}$$

$$\frac{d}{dt}\left(\frac{\partial L}{\partial \dot\lambda_{nq}^*}\right) - \frac{\partial L}{\partial \lambda_{nq}^*} \;=\; 0, \tag{33}$$

are obtained by the variation of the Lagrangian

$$L = \langle\Psi_{D_1}(t)|\frac{i}{2}\left(\frac{\overrightarrow{\partial}}{\partial t} - \frac{\overleftarrow{\partial}}{\partial t}\right) - H_S|\Psi_{D_1}(t)\rangle \tag{34}$$

Explicitly,

$$\begin{aligned}
\dot\alpha_n(t) \;&=\; -\frac{1}{2}\alpha_n\sum_q(\dot\lambda_{nq}\lambda_{nq}^* - H.c.) - i\sum_m J_{nm}\alpha_m S_{nm} \\
&\quad -i\alpha_n[\sum_q \omega_q|\lambda_{nq}|^2 - \sum_q g_q\omega_q(\lambda_{nq}+\lambda_{nq}^*)], \\
\dot\lambda_{nq}(t) \;&=\; -i[\alpha_n^{-1}\sum_m J_{nm}\alpha_m S_{nm} \\
&\quad \times(\lambda_{mq}-\lambda_{nq}) + \omega_q\lambda_{nq} - g_q\omega_q].
\end{aligned} \tag{35}$$

Here

$$\begin{aligned}
S_{nm}(t) \;&=\; \exp\{\sum_q[\lambda_{nq}^*(t)\lambda_{mq}(t) \\
&\quad -\frac{1}{2}|\lambda_{nq}(t)|^2 - \frac{1}{2}|\lambda_{mq}(t)|^2]\}
\end{aligned} \tag{36}$$

is the Debye-Waller factor. The quality of the Ansatz (31) is controlled by the evaluation of the amplitude of the deviation vector as described in Refs.[40,41]. The Ansatz has been shown to accurately reproduce the single-exciton dynamics and absorption spectra of molecular aggregates over a wide range of the exciton-phonon coupling strength[40–43,50].

III. APPLICATION TO THE LIGHT-HARVESTING COMPLEX LHCII

A. Parameterization of the Hamiltonian and computational details

LHCII possesses a trimeric structure. Each monomer contains eight chlorophylls a (Chla) and six chlorophylls b (Chlb)[69]. We use the full 42×42 one-exciton Hamiltonian for the trimeric complex, whose excitation energies ϵ_m and the electronic couplings J_{nm} are taken from[47]. We explicitly consider 48 high frequency vibrational modes with moderate-to-weak electron-phonon coupling. Their frequencies ω_q, coupling strengths $\lambda_q = S_q\omega_q$ were retrieved from the available ensemble experiments as explained in Refs.[48,49]. The λ_q are supposed to be site independent, but the coupling for Chlb is 1.25 times larger than that for Chla. As is explained in Section II C, these parameters represent some characteristic values, while the parameters for a given single molecular aggregate will be distributed around these values.

The transition dipole moments $\boldsymbol{\mu}_m$ for Chla and Chlb were retrieved from crystal structures (PDB ID: 1RWT[69]). Their absolute values for Chla and Chlb are 4.0 and 3.8 Debye, respectively.

The Brownian oscillator mode in Eq. (27) accounts for the impact of the heat bath. Following Ref.[49], its spectral density (9) is taken in the Drude form

$$D(\omega) = 2\lambda_0\frac{\omega\gamma_0}{\omega^2+\gamma_0^2}, \tag{37}$$

with the parameters $\hbar\lambda_0 = 37\text{cm}^{-1}$ and $\hbar\gamma_0 = 30\text{cm}^{-1}$. These parameters correspond to an overdamped Brownian oscillator mode. The resulting lineshape function (27) is evaluated analytically[2]:

$$\begin{aligned}
g(t) \;&=\; \frac{\lambda_0}{\gamma_0}\{e^{-\gamma_0 t} + \gamma_0 t - 1\}\left[\cot\left(\frac{\hbar\gamma_0}{2k_BT}\right) - i\right] \\
&\quad +4k_BT\frac{\lambda_0\gamma_0}{\hbar}\sum_{k=1}^{\infty}\frac{e^{-\nu_k t}+\nu_k t - 1}{\nu_k(\nu_k^2-\gamma_0^2)},
\end{aligned} \tag{38}$$

$\nu_k = (2\pi k_BT)k/\hbar$ being the Matsubara frequencies.

We assume that the pulses have Gaussian envelopes

$$E(t) = \exp\{-\Gamma^2 t^2\}, \tag{39}$$

where $\Gamma = 2\sqrt{\ln 2}/\tau_p$ and τ_p is the pulse duration (full width at half maximum of the amplitude). We set $\tau_p =$ 15 fs, as in the experiment of Ref.[16]. Following[16], the carrier frequencies of the two pump pulses are taken to be in resonance with the Chlb and Chla bands of the linear absorption spectrum of Q_y band of LHCII: $\omega_1 = 15375$ cm^{-1} and $\omega_2 = 14800$ cm^{-1} (see Ref.[44]).

For Gaussian pulses, integration over t in Eq. (22) can be done analytically, with the result

$$S(\tau) \sim \text{Re}\int_0^\infty dt_1 A(\tau,t_1)R(t_1) \tag{40}$$

where

$$\begin{aligned}
A(\tau,t_1) = e^{-\Gamma^2 t_1^2/2}\left(e^{i\omega_1 t_1 + i\omega_2 t_1}\right) + e^{-\omega^2/(2\Gamma^2)}e^{i\Omega t_1}\times \\
\left(e^{-\Gamma^2(\tau-t_1)^2/2}e^{-i(\phi-\omega\tau)} + e^{-\Gamma^2(\tau+t_1)^2/2}e^{i(\phi-\omega\tau)}\right)
\end{aligned} \tag{41}$$

and

$$\Omega = (\omega_1+\omega_2)/2,\; \omega = (\omega_2-\omega_1)/2. \tag{42}$$

The numerical evaluation of $R(t)$ through the Davydov Ansatz $|\Psi_{D_1}(t)\rangle$ requires the solution of thousands of coupled differential equations (35). We overcome the memory and computational limitations by using a GPU (Graphics Processing Unit) implementation, for which the computation time scales inversely with the number of cores on a single GPU (cf. Ref.[70]). The numerical integration of the equations of motion for the variational parameters are performed on a NVIDIA Tesla M2050 GPU with 448 processors and 2GB ECC-protected on-board memory. With our efficient GPU algorithm, the computation of the time evolution of $S(\tau)$ up to 400 fs on a single GPU requires ~ 1 hour.

B. Single-molecule response functions

It is useful to discuss the response functions $R(t)$ first. $R(t)$ defined by Eq. (26) is a product of the relaxation term $\exp\{-g(t)\}$, which is responsible for the bath-induced relaxation, and the system contribution, describing the coherent dynamics in the singly-excited excitonic manifold. The latter is governed by the system Hamiltonian H_S of Eq. (3), which comprises 42 electronic states and 48 vibrational modes. Despite the complexity of H_S, it is possible to rationalize the influence of the electron-phonon coupling on the system dynamics as a polaron effect (see Appendix A).

We start our analysis from the consideration of the bath-free ($\lambda_0 = 0$) response functions and consider Fig. 1, which shows the real part of $R(\tau)$ (left column) and its power spectrum $|R(\omega)|^2$ (right column). Panels (a) correspond to the electron-phonon coupling strengths S_q from[48,49], panels (b) correspond to $S_q/2$, and panels (c) correspond to $S_q = 0$[71].

Since the bath-induced relaxation is neglected, the $R(t)$ of Fig. 1 reflect the dynamics governed by the system Hamiltonian H_S. Hence the peaks in the power spectra $|R(\omega)|^2$ in panels (a) and (b) feature those electron-vibrational (vibronic) eigenvalues of H_S, which contribute significantly to the linear response function due to the favorable Franck-Condon factors. The $|R(\omega)|^2$ presented in panel (c) shows purely electronic eigenvalues.

A brief comparison of the peak structure of $|R(\omega)|^2$ in panels (a), (b), and (c) reveals no substantial qualitative differences. This means that the peaks have predominantly electronic origin, while the electron-vibrational coupling shifts their positions and changes their shapes. Due to the complexity of H_S and the lack of symmetry, it is impossible to assign the peak positions to any specific vibrational frequencies ω_q or parameters of the excitonic Hamiltonian $H_{\rm ex}$. Yet, the shift of the peaks of $|R(\omega)|^2$ to the blue with the decrease of the electron-phonon coupling is a polaron effect explained per Eqs. (A1) and (A3). The strongest peaks of $|R(\omega)|^2$ in panels (a) are positioned at 14820 and 15410 cm^{-1}. These values correspond to the maxima of Chla and Chlb absorption of Q_y band of LHCII, since the exciton-vibrational coupling in the LHCII Hamiltonian is optimized to reproduce the linear absorption spectrum.

In the time domain, $R(t)$ (left column of Fig. 1) exhibits rather irregular beatings with decreasing amplitudes, which reflect superpositions of multiple oscillations with incommensurable frequencies. The frequencies in the interval $[14000, 16000]$ cm^{-1} yield oscillation periods in the range $[2.08, 2.38]$ fs. Hence $R(t)$ exhibits fast oscillations with a period of ~ 2 fs. Slower oscillations of $R(t)$ on the timescale of several dozens of femtoseconds and longer are beatings.

While $|R(\omega)|^2$ has a multi-frequency structure, it is possible to single out three strongest peaks positioned at 14640, 14820, and 15410 cm^{-1} (full electron-phonon coupling S_q, panel (a)), 14860, 15000, and 15730 cm^{-1} ($S_q/2$, panel (b)), 14920, 15100, and 15830 cm^{-1} ($S_q = 0$, panel (c)). The differences of the frequencies of the third and second peaks yield periods of 56, 46, and 46 fs. These values correlate with the first maxima of $R(t)$ corresponding to 53 fs (a), 47 fs (b), and 44 fs (c). The subsequent recurrences of $R(t)$ have smaller amplitudes. For $R(t)$ of panels (b) and (c) they correspond, approximately, to multiple values of the above periods. The oscillations of $R(t)$ in panel (a) are less regular. The differences of the frequencies of the first and second peaks of $|R(\omega)|^2$ yield on oscillation period of ~ 200 fs, which correlates with the second recurrence of $R(t)$ around 250 fs.

Fig. 2 illustrates the influence of the bath on the single-molecule response. It shows the real part of $R(\tau)$ (left column) and $|R(\omega)|^2$ (right column) computed at a temperature of 77 K. In the frequency domain, the effect of the bath is to broaden and shift the vibronic peaks, so that $|R(\omega)|^2$ develops a clear three-peak structure. The peaks correspond to 14640, 14800, and 15390 cm^{-1} (a), 14840, 15000, and 15710 cm^{-1} (b), 14920, 15060, and 15810 cm^{-1} (c). In the time domain, the bath significantly quenches the amplitudes of the oscillations of $R(\tau)$ at a time scale of ~ 300 fs. The position of the first hump of $R(\tau)$ correlates with the energy difference between the two largest peaks in $|R(\omega)|^2$. They are 57 fs and 590 cm^{-1} (a), 47 fs and 710 cm^{-1} (b), 44 fs and 750 cm^{-1} (c). Hence the electron-vibrational coupling increases the oscillation period, a trend illustrated by Eq. (A5) in Appendix A.

Fig. 3 shows the real part of $R(\tau)$ (left column) and $|R(\omega)|^2$ (right column) at a temperature of 300 K. The general trends in the behavior of the single-molecule response function are those for Fig. 2. $|R(\omega)|^2$ exhibits two broadened peak at 14800, and 15360 cm^{-1} (a), 15000, and 15670 cm^{-1} (b), 15060, and 15790 cm^{-1} (c). In comparison of Fig. 2, the left peaks retain their positions, but the right peaks become a few dozens of inverse centimeters red-shifted. In the time domain, $R(\tau)$ decays within ~ 100 fs. The energy differences between the two peaks of $|R(\omega)|^2$ yield in the time domain 60 (a), 50 (b), and 46 fs (c). These times correlate with the position of the first hump of $R(\tau)$, except of panel (a) which does not exhibit any clear maximum.

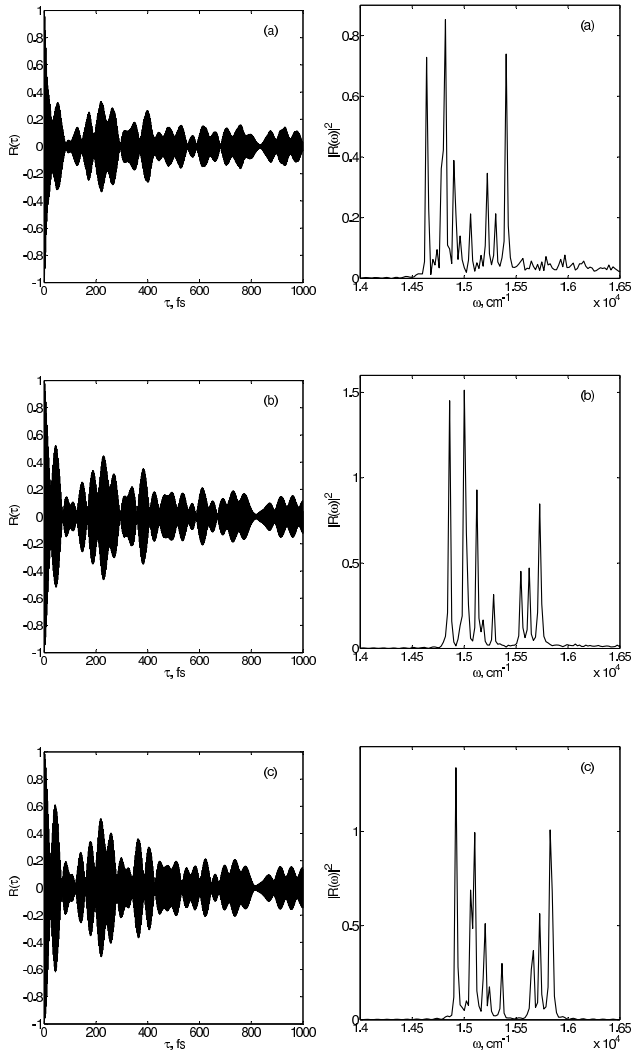

FIG. 1: The real part of the single-molecule response function $R(\tau)$ (left column) and its power spectrum $|R(\omega)|^2$ (right column) without heat bath and for $\boldsymbol{e} \parallel Z$. Panels (a) correspond to the electron-phonon coupling strengths S_q from[48,49], panels (b) correspond to $S_q/2$, and panels (c) correspond to $S_q = 0$.

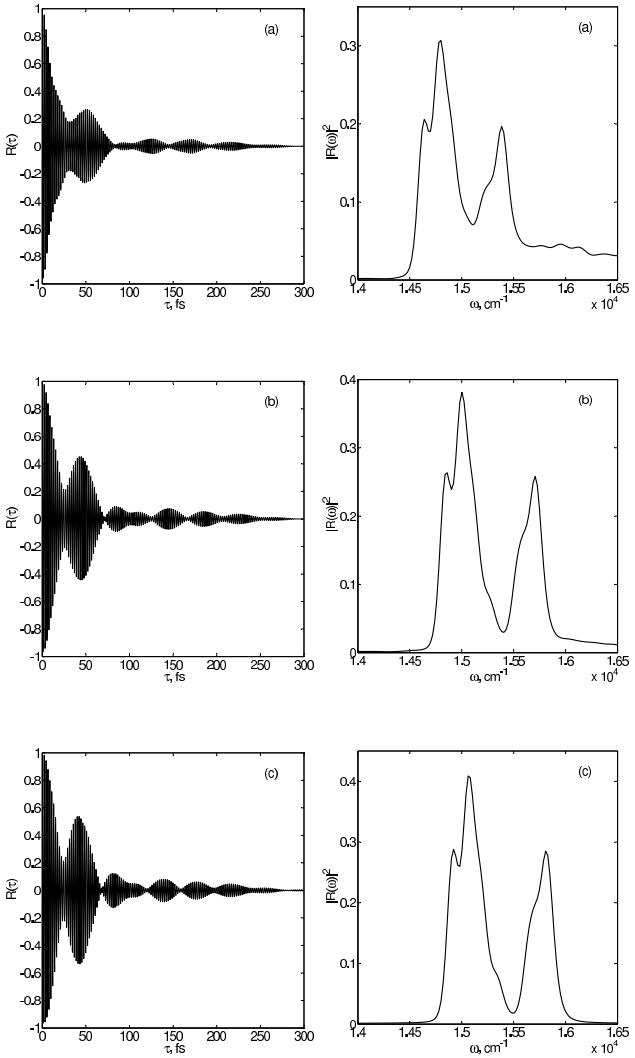

FIG. 2: The real part of the single-molecule response function $R(\tau)$ (left column) and its power spectrum $|R(\omega)|^2$ (right column) for a heat bath at 77 K and $\boldsymbol{e} \parallel Z$. Panels (a) correspond to the electron-phonon coupling strengths S_q from[48,49], panels (b) correspond to $S_q/2$, and panels (c) correspond to $S_q = 0$.

To summarize, the results of the present section give an overview of the behavior of the linear response for the parameters retrieved from ensemble experiments.

C. Single-molecule signals

We start from a simple general analysis. Eq. (41) shows that the signal $S(\tau)$ consists of a τ-independent background (the system interacts twice with the same pump pulse) and a τ-dependent contribution (the system interacts once with pump #1 and once with pump #2). Obviously, it is the latter contribution which delivers information on the single-molecule dynamics.

Eq. (41) also reveals that the dependence of the signal on the relative phase ϕ of the two pump pulses is trivial and bears no dynamic information: For any fixed τ, the signal exhibits a cosine-like behavior when ϕ is varied from 0 to 2π, in agreement with Ref.[16]. In the simulations, we assume that the pulses possess the same waveform and put $\phi = 0$. This choice renders the pulses 1 and 2 equivalent, hence $S(\tau) = S(-\tau)$.

The present section seeks to present a general qualitative picture of possible behaviors of femtosecond double-pump signals of single LHCII complexes. Below, we demonstrate how different realizations of the site energies

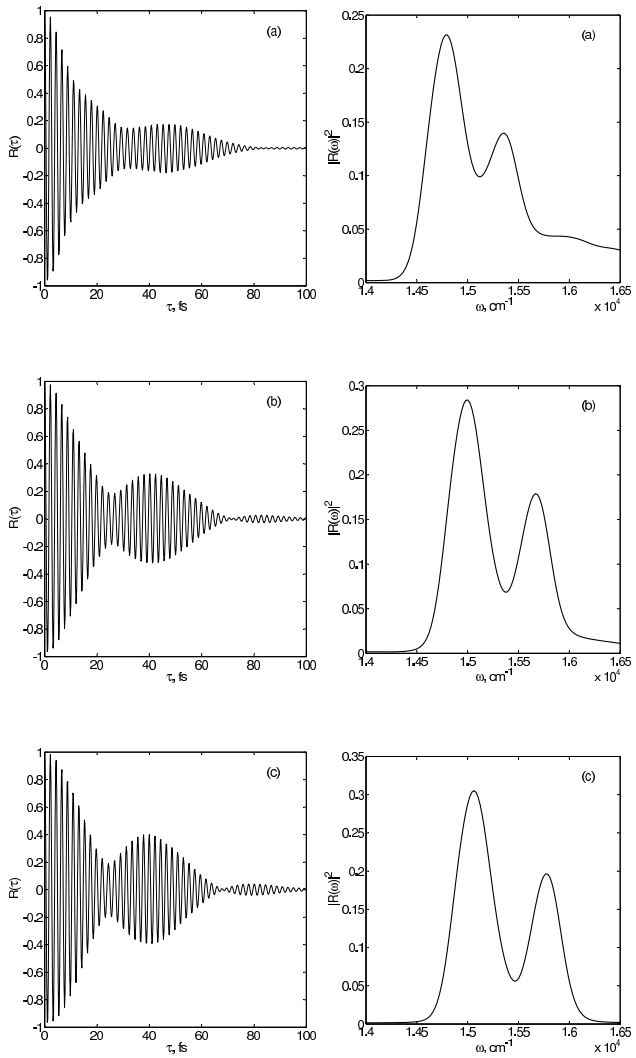

FIG. 3: The real part of the single-molecule response function $R(\tau)$ (left column) and its power spectrum $|R(\omega)|^2$ (right column) for a heat bath at 300 K and $\boldsymbol{e} \parallel Z$. Panels (a) correspond to the electron-phonon coupling strengths S_q from[48,49], panels (b) correspond to $S_q/2$, and panels (c) correspond to $S_q = 0$.

ϵ_m, the electron-phonon couplings χ_{qm}, the system-bath couplings κ_j, and the transition dipole moment orientations and $\boldsymbol{\mu}_n$ affect the signal.

Fig. 4 shows the single-molecule signal $S(\tau)$ for different electron-phonon coupling strengths. Panel (a) corresponds to Huang-Rhys factors S_q retrieved from Refs.[48,49], panel (b) corresponds to $S_q/2$, and panel (c) corresponds to $S_q = 0$. The two pump pulses are polarized along the Z axis of the laboratory frame ($\boldsymbol{e} \parallel Z$). The bath is specified by the lineshape function of Eq. (38) at temperature $T = 77$ K (left column) and $T = 300$ K (right column).

The signals in Fig. 4 exhibit beatings with a single frequency. The transients in panels (a) oscillate with a period ~ 58 fs which corresponds to the difference of the carrier frequencies of the pump pulses $\omega_1 - \omega_2$. The oscillation period decreases with decreasing electron-phonon coupling: ~ 36 fs (panel (b)) and ~ 28 fs (panel (c)). Section III B offers a clear understanding of the origin of these beatings. Eq. (40) reveals that the (time-dependent part) of the single-molecule signal $S(\tau)$ induced by short and temporally well separated pulses is proportional to $R(\tau)e^{i\omega_2\tau}$. Hence the frequency of the oscillations of $S(\tau)$ is given by the difference of $\omega_2 = 14800$ cm^{-1} and the frequency of the rightmost peak of $|R(\omega)|^2$ in Figs. 2 and 3. Qualitatively, a decrease of the oscillation period with the decrease of the electron-phonon coupling is a polaron effect as explained in Appendix A.

Fig. 4 reveals that the electron-vibrational coupling affects the single-molecule transients significantly. The beatings shown in Fig. 4 are thus of mixed electron-vibrational (vibronic) origin. The oscillatory responses detected in ensemble two-dimensional photon-echo signals of various molecular aggregates seem also be caused by beatings between several vibronic states involved (see the discussion in Ref.[72,73] and references therein). The oscillations in the single-molecule signals depicted in Fig. 4 survive the bath-induced relaxation. As expected, the quenching rate increases with the bath temperature: the oscillations last for ~ 300 fs at 77 K, but only for ~ 100 fs at 300 K.

There exist two qualitative differences between the signals depicted in Fig. 4 for LHCII and those reported in Ref.[16] for LH2: The latter exhibit oscillations with characteristic periods within $100 - 200$ fs and show no visible damping on a time scale of ~ 400 fs. To address these differences and to reveal how the variation of the system-bath coupling affects the single-molecule responses, Fig. 5 shows the signals presented in Fig. 4, but calculated for zero system-bath coupling ($\kappa_j = 0$, $\lambda_0 = 0$). The signals exhibit fast underdamped oscillations superimposed by slower beatings. For each of the panels (a), (b) and (c), the periods of fast oscillations in Figs. 4 and 5 are the same. The oscillation periods of the slower beatings also decrease with decreasing electron-phonon couplings. They are ~ 250 fs (panel (a)), ~ 150 fs (panel (b)), and ~ 120 fs (panel (c)). The "remnants" of these beatings are seen in the left column of Fig. 4. The behavior of the signals in Fig. 5 is immediately deduced from that of the response functions depicted in Fig. 1, since $S(\tau) \approx R(\tau)e^{i\omega_2\tau}$. The decrease of the periods of fast and slow beatings with decreasing electron-phonon couplings can be rationalized as a polaron effect (see Appendix A).

The signals reported in Ref.[16] for LH2 also exhibit undamped oscillations on the time scale of several hundreds of femtoseconds. We tentatively conclude that the bath parameters, optimized to reproduce ensemble experiments, overestimate the effect of homogeneous broadening. The actual system-bath coupling might be significantly weaker, while the effect of inhomogeneous broad-

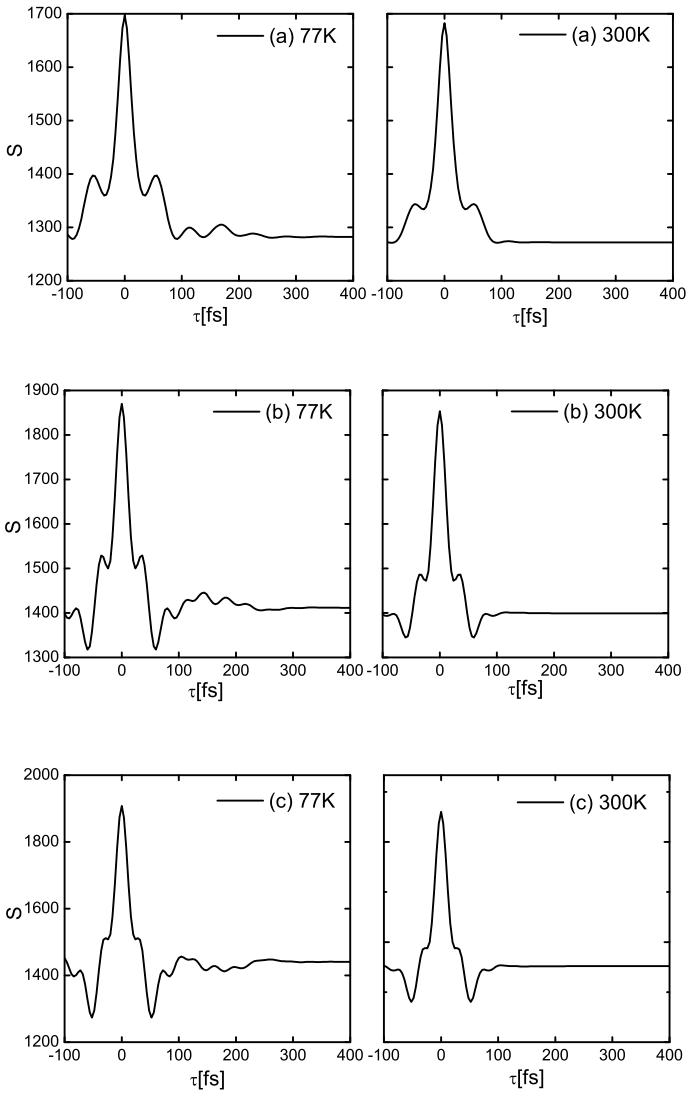

FIG. 4: Single-molecule signal $S(\tau)$ for $\boldsymbol{e} \parallel Z$. The heat bath is at 77 K (left column) and at 300 K (right column). Panels (a) correspond to the electron-phonon coupling strengths S_q from[48,49], panels (b) correspond to $S_q/2$, and panels (c) correspond to $S_q = 0$.

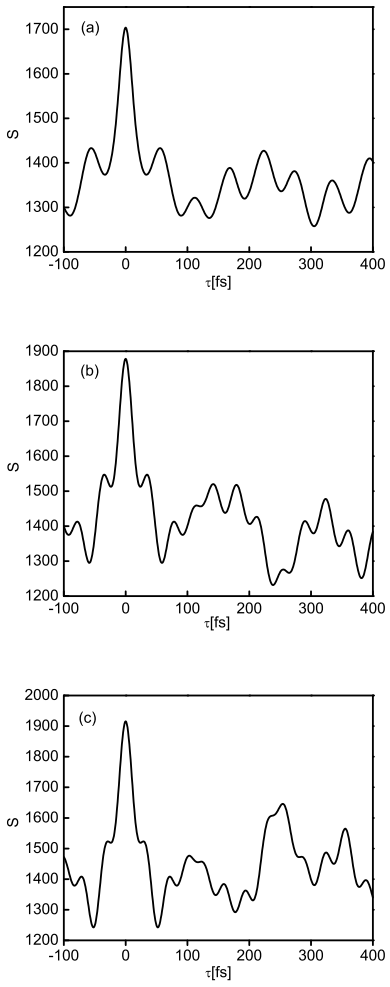

FIG. 5: Single-molecule signal $S(\tau)$ for $\boldsymbol{e} \parallel Z$ without heat bath. Panels (a) correspond to the electron-phonon coupling strengths S_q from[48,49], panels (b) correspond to $S_q/2$, and panels (c) correspond to $S_q = 0$.

ening (static disorder) may be more pronounced than estimated from the ensemble experiments.

The signals of Ref.[16] do not exhibit fast oscillations with a period of several tens of femtoseconds. However, such oscillations may not be detectable with the time resolution of these experiments.

Next, we consider the effect of single-molecule orientation. Fig. 6 shows $S(\tau)$ calculated at $T = 77$ K (a) and $T = 300$ K (b) for the polarization $\boldsymbol{e}$ of the pump pulses directed along the axis X, Y, and Z of the laboratory frame (the legends XX, YY, and ZZ, respectively). The orientation-averaged signal, which corresponds to the replacement of the geometrical factor (28) by the averaged factor (29), is also presented in the figure.

The signals calculated for different $\boldsymbol{e}$, as well as the averaged signal, exhibit similar oscillatory behavior, although the amplitudes of the beatings are different. The observed weak sensitivity of the signals to specific molecular orientation can be understood as follows. As a whole, LHCII has no preferential orientations of the transition dipole moments $\boldsymbol{\mu}_m$ in certain directions or in certain planes in the molecular frame. In a first approximation, it is almost isotropic, hence a low polarization sensitivity. LH2, on the other hand, has a double-ring structure. Hence, in-ring and out-of-ring directions differ considerably. The single-molecule transients of LH2 indeed seem to exhibit more pronounced anisotropy effects[16].

Finally, we analyze how the spread in the site energies ϵ_m affects the single-molecule signals. The site-energy disorder is believed to be caused by the slowest fluctuations of the pigment-protein environment and is a ma-

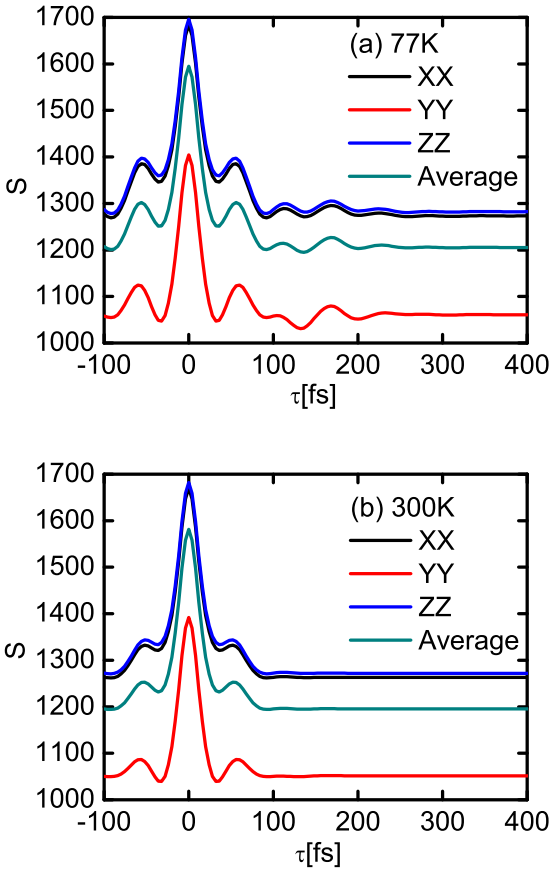

FIG. 6: $S(\tau)$ for different polarization of the pump pulses in the laboratory frame (see text for details). The system and the bath parameters are the same as for Fig. 4(a)

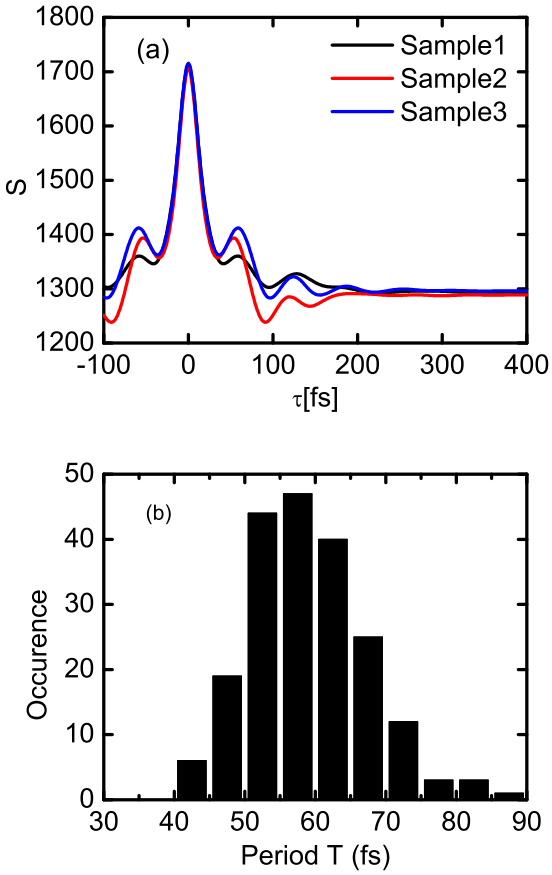

FIG. 7: (a) Single-molecule signal for three representative LHCII samples at 77K. (b) Histogram of the oscillation period T retrieved from 200 samples. The system and the bath parameters are the same as for Fig. 4(a)

jor contribution to the static (inhomogeneous) disorder in ensemble experiments[74–76]. A single-molecule experiment selects a specific disordered molecular configuration.

Fig. 7(a) shows three representative $S(\tau)$ of LHCII at 77 K. They correspond to random realizations of the site energies ϵ_m which are sampled from uncorrelated Gaussian distributions with a standard deviation of 80 cm^{-1} for Chls a and 104 cm^{-1} for Chls b[77,78]. All three signals exhibit similar oscillatory behavior (cf. Fig. 4(a)), but the oscillation periods are different. To quantify these differences, we retrieved the oscillation periods from 200 samplings of $S(\tau)$. The resulting histogram (Fig. 7(b)) features a wide distribution of periods between $\sim$ 40 fs and $\sim$ 90 fs with a maximum near 58 fs. The spread of the periods extracted from the single-molecule signals measured in Ref.[16] is even broader. Heterogeneity of electronic couplings between the chlorophyll molecules[75,76] may result in additional broadening of the distribution.

IV. CONCLUSION

Inspired by recent experiments of the van Hulst group[14–16], we have developed a first principles theoretical description of femtosecond double-pump single-molecule signals of molecular aggregates. All singly-excited electronic states and vibrational high-frequency modes with significant electron-vibrational couplings have been incorporated in the system Hamiltonian. The system dynamics is described within the Davydov D_1 Ansatz. The remaining intra- and inter-molecular vibrational modes are treated as a heat bath and their effect is accounted for through the lineshape functions.

We have applied the theory to simulate femtosecond double-pump signals of single LHCII complexes. The use of the GPU implementation and an efficient algorithm permitted us to reduce the computation time of each signal up to 400 fs on a single GPU to $\sim$ 1 hour. The calculated signals exhibit pronounced oscillations of vibronic origin, in qualitative agreement with the results of Ref.[16] for LH2. The period of these oscillations de-

creases with decreasing electron-vibrational couplings.

Both the ensemble linear absorption spectra and single-molecule double-pump signals are determined by linear response functions. However, the single-molecule signal is not subject to inhomogeneous broadening and delivers information on snapshot values of the parameters specifying the system Hamiltonian. The simulation and interpretation of individual femtosecond responses of molecular aggregates may require the refinement of the existing microscopic models optimized to reproduce ensemble experiments. For example, the existing models may overestimate the strength of the system-bath coupling (homogeneous broadening), while underestimating static disorder (inhomogeneous broadening).

The double-pump experiment on single LH2 molecules reported in Ref.[16] involves weak laser pulses. Such experiments monitor the dynamics of electronic coherences of the system density matrix. The use of stronger laser pulses may permit to simultaneously follow evolutions of both electronic populations and coherences[17]. Future single-molecule experiments may shed additional light on the actively debated topic of quantum effects in biology, which may have implications for a large variety of phenomena, from light harvesting to consciousness[79–83].

Acknowledgments

Support from the Singapore National Research Foundation through the Competitive Research Programme (CRP) under Project No. NRF-CRP5-2009-04 is gratefully acknowledged. M.F.G. and W.D. acknowledge support from the Deutsche Forschungsgemeinschaft through the DFG-Cluster of Excellence "Munich-Centre for Advanced Photonics" (www.munich-photonics.de). M.F.G. thanks all the members of the Yang Zhao group for hospitality and numerous stimulating discussions.

APPENDIX A: A PEDESTRIAN ANALYSIS OF POLARON EFFECTS

In a first approximation, the electron-phonon coupling renormalizes the site energies and electronic couplings in the excitonic Hamiltonian as follows (see, e.g., Ref.[84]):

$$\tilde{\epsilon}_m = \epsilon_m + r_m, \tag{A1}$$

$$\tilde{J}_{nm} = J_{nm}\theta_n\theta_m \tag{A2}$$

where

$$r_m = -\sum_q |\chi_{qm}|^2, \tag{A3}$$

$$\theta_m = e^{-\frac{1}{2}\sum_q \coth\left(\frac{\hbar\omega_q}{2k_BT}\right)|\chi_{qm}|^2}. \tag{A4}$$

Eqs. (A1) and (A3) reveal that the electron-vibrational coupling decreases the site energies. If, furthermore, the coupling is site-independent ($\chi_{qm} \approx \chi_q$, as is approximately the case for the present model of LHCII), then all $\tilde{\epsilon}_m$ decrease by the same value $r_m = r$. Hence the kth eigenvalues $\tilde{\mathcal{E}}_k$ of the renormalized excitonic Hamiltonian $\tilde{H}_{\rm ex}$ are red-shifted in comparison with the kth eigenvalues $\mathcal{E}_k$ of the purely excitonic Hamiltonian $H_{\rm ex}$.

Eqs. (A2) and (A4) show that the electron-vibrational coupling decreases the effective electronic coupling. We argue that this effect should decrease (on the average) the differences between the neighboring eigenvalues of the excitonic Hamiltonian,

$$|\tilde{\mathcal{E}}_k - \tilde{\mathcal{E}}_{k'}| < |\mathcal{E}_k - \mathcal{E}_{k'}|. \tag{A5}$$

We cannot prove Eq. (A5) in full generality, but we demonstrate that it holds in two particular cases. Let us select a dimer comprised of the sites 1 and 2 with the coupling J_{12} and neglect the coupling of the dimer to the other sites. Then, given $r_1 = r_2 = r$, we have

$$|\tilde{\mathcal{E}}_2 - \tilde{\mathcal{E}}_1| = \sqrt{(\epsilon_1 - \epsilon_2)^2 + 4\tilde{J}_{12}^2}, \tag{A6}$$

which proves Eq. (A5). For a molecular ring comprising N sites with only const nearest-neighbor coupling J and same site energy $\epsilon_n = \epsilon$, we have (see, e.g., Ref.[85])

$$|\tilde{\mathcal{E}}_k - \tilde{\mathcal{E}}_{k'}| = 2\tilde{J}|\cos\left(\frac{2\pi k}{N}\right) - \cos\left(\frac{2\pi k'}{N}\right)|, \tag{A7}$$

with $k, k' = 0, 1, ..., N-1$. Thus Eq. (A5) holds.

[1] A. H. Zewail, J. Phys. Chem. A **104**, 5660 (2000).
[2] S. Mukamel, *Principles of Nonlinear Optical Spectroscopy* (Oxford University Press, New York, 1995).
[3] M. Cho, *Two-Dimesional Optical Spectroscopy* (CRC Press, New York, 2009).
[4] L. Valkunas, D. Abramavicius, T. Mančal, *Molecular Excitation Dynamics and Relaxation* (Wiley-VCH, Weinheim, 2013).
[5] *Coherent Multidimensional Optical Spectroscopy.* Special Issue of Acc. Chem. Res., Vol. 42, No 9 (2009).
[6] W. E. Moerner and L. Kador, Phys. Rev. Lett. **62**, 2535 (1989).
[7] M. Orrit and J. Bernard, Phys. Rev. Lett. **65**, 2716 (1990).
[8] A. M. van Oijen, M. Ketelaars, J. Köhler, T.J. Aartsma, and J. Schmidt, Science **285**, 400 (1999).
[9] M. A. Bopp, A. Sytnik, T. D. Howard, R. J. Cogdell, and

R. M. Hochstrasser, Proc. Natl. Acad. Sci. U. S. A. **96**, 11271 (1999).
[10] S. Mackowski, S. Wörmke, T. H. P. Brotosudarmo, H. Scheer, and C. Brauchle, Photosynth. Res. **95**, 253 (2008).
[11] G. S. Schlau-Cohen, Q. Wang, J. Southall, R. J. Cogdell, and W. E. Moerner, Proc. Natl. Acad. Sci. U. S. A. **110**, 10899 (2013).
[12] S. Tubasum, R. Camacho, M. Meyer, D. Yadav, R. J. Cogdell, T. Pullerits, and I.G. Scheblykin, Phys. Chem. Chem. Phys. **15**, 19862 (2013).
[13] J. Chmeliov, L. Valkunas, T. P. J. Krüger, C. Ilioaia, S. Tubasum, R. Camacho, M. Meyer, D. Yadav, R. J. Cogdell, T. Pullerits, and R. van Grondelle, New J. Phys. **15**, 085007 (2013).
[14] D. Brinks, R. Hildner, E. M. H. P. van Dijk, F. D. Stefani, J. B. Nieder, J. Hernandof, and N. F. van Hulst, Chem. Soc. Rev. **43**, 2476 (2014).
[15] R. Hildner, D. Brinks, F. D. Stefania, and N. F. van Hulst, Phys. Chem. Chem. Phys. **13**, 1888 (2011).
[16] R. Hildner, D. Brinks, J. B. Nieder, R.J. Cogdell, and N. F. van Hulst, Science **340**, 1448 (2013).
[17] M. F. Gelin, Y. Tanimura, and W. Domcke, J. Chem. Phys. **139**, 214302 (2012).
[18] M. F. Gelin, D. Egorova, and W. Domcke, J. Phys. Chem. B **115**, 5648 (2011).
[19] M. F. Gelin, D. Egorova, and W. Domcke, Phys. Chem. Chem. Phys. **15**, 8119 (2013).
[20] T. Renger, V. May, and O. Kühn. Phys. Rep. **343**, 137 (2001).
[21] S. Mukamel and D. Abramavicius, Chem. Rev. **104**, 2073 (2004).
[22] R. van Grondelle and V. I. Novoderezhkin, Phys. Chem. Chem. Phys. **8**, 793 (2006).
[23] A. Ishizaki and G. R. Fleming, J. Chem. Phys. **130**, 234110 (2009).
[24] A. Ishizaki and G. R. Fleming, J. Chem. Phys. **130**, 234111 (2009).
[25] Y. Tanimura, J. Phys. Soc. Jpn. **75**, 082001 (2006).
[26] M. H. Beck, A. Jäckle, G. A. Worth, and H. D. Meyer, Phys. Rep. **324**, 1 (2000) .
[27] H. D. Meyer, Comput. Mol. Sci. **2**, 351 (2012).
[28] H. Wang and M. Thoss, Chem. Phys. **347**, 139 (2008).
[29] K. H. Hughes, C.D. Christ, and I. Burghardt, J. Chem. Phys. **131**, 024109 (2009).
[30] K. H. Hughes, C.D. Christ, and I. Burghardt, J. Chem. Phys. **131**, 124108 (2009).
[31] J. Prior, A. W. Chin, S. F. Huelga, and M. B. Plenio, Phys. Rev. Lett. **105**, 050404 (2010). Y. Yao, L. W. Duan, Z. G Lu, C. Q. Wu, and Y. Zhao, Phys. Rev. E **88**, 023303 (2013)
[32] R. Doll, D. Zueco, M. Wubs, S. Kohler, and P. Hänggi, Chem. Phys. **347**, 243 (2008).
[33] M. F. Gelin, D. Egorova, and W. Domcke, Phys. Rev. E **84**, 041139 (2011).
[34] A. S. Davydov and N. I. Kislukha, Phys. Status Solidi B **59**, 465 (1973).
[35] A. S. Davydov, *Solitons in Molecular Systems* (Reidel, Dordrecht, 1985).
[36] M. J. Šrinjar, D. V. Kapor, and S. D. Stojanović, Phys. Rev. A **38**, 6402 (1988).
[37] L. Cruzeiro-Hansson, Phys. Rev. Lett. **73**, 2927 (1994).
[38] Y. Yao and Y. Zhao, J. Chem. Phys. **139**, 014102 (2013).
[39] N. Wu, L.W. Duna, X. Li and Y. Zhao, J. Chem. Phys. **138**, 084111 (2013).
[40] J. Sun, B. Luo, and Y. Zhao, Phys. Rev. B **82**, 014305 (2010).
[41] B. Luo, J. Ye, C. B. Guan, and Y. Zhao, Phys. Chem. Chem. Phys. **12**, 15073 (2010).
[42] G.C. Yang, N. Wu, T. Chen, K.W. Sun, and Y. Zhao, J. Phys. Chem. C **116**, 3747 (2012).
[43] J. Ye, K. W. Sun, Y. Zhao, Y. J. Yu, C. K. Lee, and J. S. Cao, J. Chem. Phys. **136**, 245104 (2012). K. W. Sun, J. Ye, and Y. Zhao, J. Chem. Phys. **141**, 124103 (2014).
[44] H. van Amerogen, L. Valkunas, and R. van Grondelle, *Photosynthetic Excitons* (World Scientific, Singapore, 2000).
[45] T. P. J. Krüger, V. I. Novoderezhkin, C. Ilioaia, and R. van Grondelle, Biophys. J. **98**, 3093 (2010).
[46] G. S. Schlau-Cohen, A. Ishizaki, T. R. Calhoun, N. S. Ginsberg, M. Ballottari, R. Bassi, and G. R. Fleming, Nat. Chem. **4**, 389 (2012).
[47] V. I. Novoderezhkin, A. Martin, and R. van Grondelle, Phys. Chem. Chem. Phys. **13**, 17093 (2011).
[48] V. I. Novoderezhkin, M. A. Palacios, H. van Amerongen, and R. van Grondelle. J. Phys. Chem. B **109**, 10493 (2005).
[49] V. I. Novoderezhkin, M. A. Palacios, H. van Amerongen, and R. van Grondelle. J. Phys. Chem. B **108**, 10363 (2004).
[50] T. D. Huynh, K. W. Sun, M. Gelin, and Y. Zhao, J. Chem. Phys. **139**, 104103 (2013).
[51] M. F. Gelin, L. Z. Sharp, D. Egorova, and W. Domcke, J. Chem. Phys. **136**, 034507 (2012).
[52] T. Renger, A. Klinger, F. Steinecker, M. Schmidt am Busch, J. Numata, and F. Müh, J. Phys. Chem. B **116**, 14565(2012).
[53] T. Renger, F. Müh, Phys. Chem. Chem. Phys. **15**, 3348(2013).
[54] V. Butkus, L. Valkunas, and D. Abramavicius, J. Chem. Phys. **140**, 034306 (2014).
[55] G. S. Schlau-Cohen, S. Bockenhauer, Q. Wang, and W. E. Moerner, Chem. Sci. **5**, 2933 (2014).
[56] N. F. Scherer, R. J. Carlson, A. Matro, Mei Du, A. J. Ruggiero, V. Romero Rochin, J. A. Cina, G. R. Fleming, and S. A. Rice, J. Chem. Phys. **95**, 1487 (1991).
[57] N. F. Scherer, A. Matro, L. D. Ziegler, M. Du, R. J. Carlson, J. A. Cina, and G. R. Fleming, J. Chem. Phys. **96**, 4180 (1992).
[58] S. Mukamel and M. Richter, Phys. Rev. A **83**, 013815 (2011).
[59] M. F. Gelin, A. V. Pisliakov, and W. Domcke, Phys. Rev. A **65**, 062507 (2002).
[60] Recently, several groups have performed fluorescence-detected four-wave mixing ensemble experiments, which are designed to probe small amounts of molecules and permit thus to diminish inhomogeneous broadening (see[61] and references therein). First single-molecule four-wave mixing signals have also been measured[62]. These experiments can be described by the third order response functions, which were constructed in Ref.[50] using the Davydov Ansätze.
[61] A. K. De, D. Monahan, J. M. Dawlaty, and G. R. Fleming, J. Chem. Phys. **140**, 194201 (2014).
[62] D. Brinks, R. Hildner, F. D. Stefani, and N. F. van Hulst, Faraday Discuss. **153**, 51 (2011).
[63] H. Dong and G. R. Fleming, J. Phys. Chem. B **117**, 11318 (2013).
[64] Otherwise $C_{n,n'}$ should be substituted by the time-dependent orientational correlation functions, which can be evaluated in different models (see, e.g. Ref.[65] and refer-

ences therein).
[65] M. F. Gelin and D. S. Kosov, J. Chem. Phys. **124**, 144514 (2006).
[66] In practice, it is more efficient to perform the orientational sampling in the molecular frame (see[67] for more details). In this frame, all $\boldsymbol{\mu}_n$ are fixed, but $\boldsymbol{e}$ are randomly distributed in space. The result of the averaging is invariant with respect to the choice of a particular reference frame.
[67] A. P. Blokhin, M. F. Gelin, I. I. Kalosha, S. A. Polubisok, and V. A. Tolkachev, J. Chem. Phys. **110**, 978 (1999).
[68] P. A. M. Dirac, Proc. Cambridge Philos. Soc. **26**, 376 (1930); J. Frenkel, *Wave Mechanics* (Oxford University Press, New York, 1934).
[69] Z. F. Liu, H. C. Yan, K. B. Wang, T. Y. Kuang, J. P. Zhang, L. L. Gui, X. M. An, W. R. Chang. Nature **428**, 287 (2004).
[70] B. Hein, C. Kreisbeck, T. Kramer, and M. Rodriguez, New J. Phys. **14**, 023018 (2012).
[71] To illustrate the effect of the 48 system vibrational modes, we consider two additional models corresponding to $S_q/2$ and $S_q = 0$. We do not believe, of course, that the exciton-phonon couplings can vary so drastically in actual single-molecule signals. We just wish to grasp the trend.
[72] T. Mančal, N. Christensson, V. Lukeš, F. Milota, O. Bixner, H. F. Kauffmann, and J. Hauer, J. Phys. Chem. Lett. **3**, 1497 (2012).
[73] F. D. Fuller, J. Pan, A. Gelzinis, V. Butkus, S. S. Senlik, D. E. Wilcox, C. F. Yocum, L. Valkunas, D. Abramavicius, and J. P. Ogilvie, Nat. Chem. **6**, 706 (2014).
[74] D. Abramavicius, L. Valkunas, and R. van Grondelle, Phys. Chem. Chem. Phys. **6**, 3097 (2004).
[75] C. Curutchet, J. Kongsted, A. M. Losa, H. H. Nejad, G. D. Scholes, B. Mennucci. J. Am. Chem. Soc. **133**, 3078 (2011).
[76] H. W. Kim, A. Kelly, J. W. Park, Y. M. Rhee, J. Am. Chem. Soc. **134**, 11640 (2012).
[77] The values of the standard deviation were fitted to reproduce the experimental ensemble absorption spectrum of the Q_y band of LHCII at room temperature reported in Ref.[78] (not shown).
[78] K. L. Wells, P. H. Lambrev, Z. Y. Zhang, G. Garab, and H. S. Tan. Phys. Chem. Chem. Phys. **16**, 11640 (2014).
[79] A. Ishizaki and G. R. Fleming, Annu. Rev. Condens. Matter Phys. **3**, 333 (2012).
[80] N. Lambert, Y.-N. Chen, Y.-C. Cheng, C.-M. Li, G.-Y. Chen, and F. Nori, Nat. Phys. **9**, 10 (2013).
[81] J. M. Anna, G. D. Scholes and R. van Grondelle, Bioscience **64**, 14 (2014).
[82] S. Mukamel, J. Phys. Chem. A **117**, 10563 (2013).
[83] S. Hameroff and R. Penrose, Physics of Life Reviews **11**, 39 (2014).
[84] F. A. Pollock, D. P. S. McCutcheon, B. W Lovett, E. M Gauger, and A. Nazir, New J. Phys. **15**, 075018 (2013).
[85] T. Meier, Y. Zhao, V. Chernyak, and S. Mukamel, J. Chem. Phys. **107**, 3876 (1997).